IEEE Photonics Journal
An IEEE Photonics Society Publication

Open Access

# Monolithic Microlens VCSELs With High Beam Quality

Volume 9, Number 4, August 2017

Youwen Huang
Xing Zhang, *Member, IEEE*
Jianwei Zhang
Yiyang Xie
Werner Hofmann, *Member, IEEE*
Yongqiang Ning
Lijun Wang

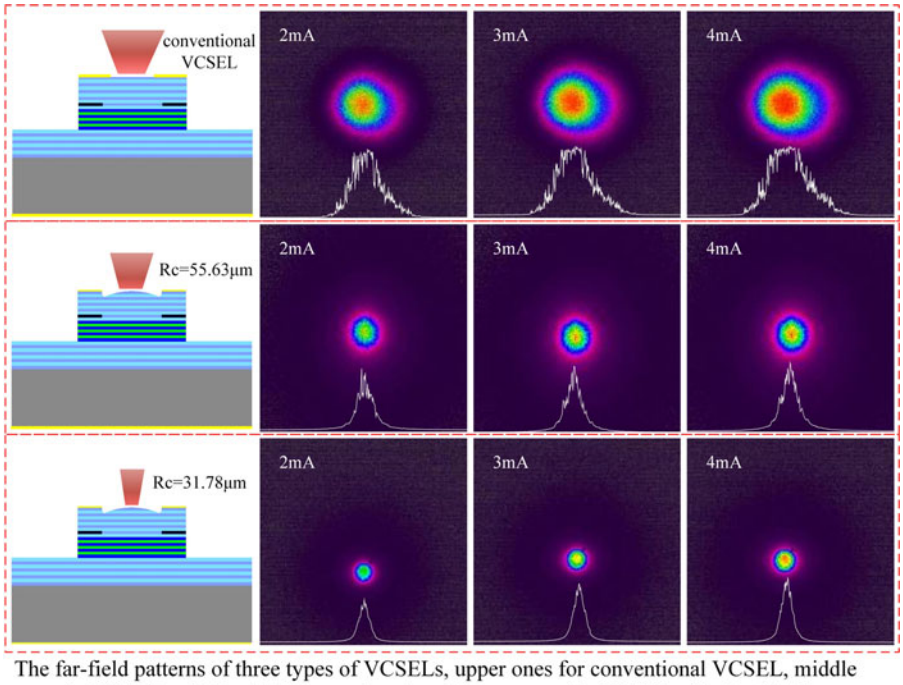


The far-field patterns of three types of VCSELs, upper ones for conventional VCSEL, middle ones for VCSEL with Rc=55.63 μm micro-lens, bottom ones for VCSEL with Rc=31.78 μm micro-lens, at injection currents of 2, 3 and 4 mA.

DOI: 10.1109/JPHOT.2017.2719702
1943-0655 © 2017 IEEE

IEEE photonics SOCIETY

IEEE

# Monolithic Microlens VCSELs With High Beam Quality

**Youwen Huang,[1,2] Xing Zhang,[1] *Member, IEEE*, Jianwei Zhang,[1] Yiyang Xie,[3] Werner Hofmann,[4] *Member, IEEE*, Yongqiang Ning,[1] and Lijun Wang[1]**

[1]State Key Laboratory of Luminescence and Applications, Changchun Institute of Optics, Fine Mechanics and Physics, Chinese Academy of Sciences, Changchun 130033, China
[2]University of Chinese Academy of Sciences, Beijing 100049, China
[3]Beijing University of Technology, Beijing 100124, China
[4]School of Solid State Physics, Technical University of Berlin, Berlin 10623, Germany

*DOI:10.1109/JPHOT.2017.2719702*


Manuscript received April 21, 2017; revised June 20, 2017; accepted June 20, 2017. Date of publication June 26, 2017; date of current version July 11, 2017. This work was supported in part by the National Natural Science Foundation of China (Grant Nos. 61434005, 61474118, 61376070, 11404326 and 11674314), in part by the Youth Innovation Promotion Association CAS (2017260), in part by the Science and Technology Program of Jilin province (20150203011GX), and in part by the Science and Technology Program of Changchun, China (15SS02). Corresponding author: Xing Zhang (e-mail: zhangx@ciomp.ac.cn).

**Abstract:** In this paper, we report on high beam quality vertical-cavity surface-emitting lasers (VCSELs) featuring a monolithically integrated aspherical microlens. This lens is fabricated by a one-step diffusion-limited wet etch process. VCSELs with microlenses with different curvature radius are designed, fabricated, and characterized, as well as reference VCSEL devices without the microlens. Significant improvement of beam divergence and single-mode performance are demonstrated in microlens VCSELs. The divergence angles of a conventional VCSEL are 14.5°, 16.0°, and 17.0° (full width at D4$\sigma$) at 2 mA, 3 mA, and 4 mA, respectively, with a $M^2$ value measured to be 6.9 at 3 mA. Under the same current injection, the divergence angles of a comparable VCSEL with a micro-lens (curvature radius of 31.8 $\mu$m) are reduced to 4.8°, 5.5°, and 5.7°, respectively. The $M^2$ value of the lensed VCSEL is as low as 1.9 at 3 mA.

**Index Terms:** Semiconductor laser, VCSEL, micro-lens, high beam quality, wet-etching.

## 1. Introduction

In the areas of fiber-optic communication, optical interconnects, high-speed lasers, printing or LiDAR, the vertical-cavity surface-emitting laser (VCSEL), as a cost- and energy- efficient source, has great application potential and market value. All these applications benefit from its inherent advantages such as longitudinal single mode emission, circular beam shape, combined with ultra-low threshold currents and power consumption. However, the intrinsic large divergence angles, poor transverse mode properties and lower beam quality of VCSELs restrict the application areas and raise the cost for beam-shaping and packaging. Many methods and technologies had been used to improve the beam quality of VCSELs, such as shallow surface relief [1], integrating surface gratings [2], anti-resonant reflecting optical wave guides [3], external cavities [4], curved dielectric mirrors [5], [6] and photonic crystal defects [7]. Yet, previous mentioned methods suffered from a sophisticated fabrication process, expensive equipment and practical problems. Microlenses monolithically integrated on the VCSEL output window is a potential method to compress

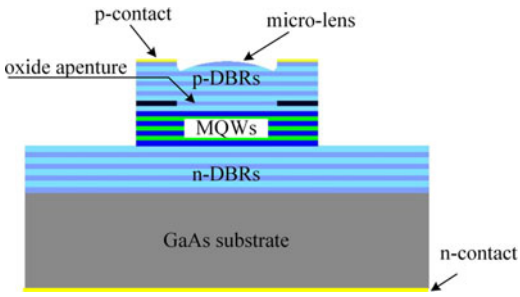


Fig. 1. The schematic cross-section of micro-lens integrated VCSEL.

far-field divergence angles and control the mode-profile simultaneously. So far, numerous methods to fabricate micro-lenses have been applied, which can be classified based on the materials forming of the micro-lens. On the one hand, the photoresist and polymer micro-lenses fabricated by thermal re-flow technology or directly laser write technology [8]–[10] and RIE/ICP etching. Though, the organic materials can't withstand the high temperatures or organic solvents, which greatly limit the practicability of this method. Micro-lenses fabricated by sputtered dielectric films and ICP/RIE etching can achieve improved VCSEL output performance [5], [6]. Nevertheless, integrating such a micro-lens into a VCSEL structure requires sophisticated sputtering and dry-etching equipment with precise process control.

In this study, a new economic and easy-to-operate micro-lens fabrication method is used to improve the divergence and single mode performance of 850 nm VCSELs. The novel micro-lens integrated VCSEL forms a small and compact monolithically integrated optical system. At first, the mode properties of VCSELs with and without micro-lens were numerically simulated. Based on the results of simulation, micro-lens designs were derived and integrated micro-lens VCSELs were fabricated. To achieve optimized divergence angles and single mode performance, the influence of the lens parameters on the VCSEL characteristics was investigated in detail.

## 2. Device Structure and Simulation

The schematic cross-section of micro-lens VCSEL is illustrated in Fig. 1. The VCSEL wafer is grown on the (100) $GaAs$ substrate by AIXTRON 200-4 metal organic chemical vapor deposition (MOCVD) and designed for operating at wavelength of 850 nm. The active layer consists of three $GaAs/AlGaAs$ quantum wells. A 30 nm thick $Al_{0.98}Ga_{0.02}As$ layer located above the *p*-type space layer is oxidized about 360 seconds at 420 °C under nitrogen gas bubbled through water at 95 °C to form current confinement apertures with diameter of 5–6 $\mu$m. The *p*-type DBR is stacked up by 23-pairs of alternative quarter-wavelength thick C-doping $Al_{0.12}Ga_{0.88}As/Al_{0.9}Ga_{0.1}As$ layers, the bottom DBR consists of 34.5-pairs of Si-doping $Al_{0.12}Ga_{0.88}As/Al_{0.9}Ga_{0.1}As$ layers.

Aspherical micro-lenses can shape the beam of VCSEL without spherical and other optical aberrations. The divergence angle compression property of the additional laser writing micro-lens was verified in ref. [10]. However, in order to improve the single mode performance we must introduce different losses for the fundamental and the higher order transverse modes. A series of numerical simulations was carried out for demonstrating the capacity of micro-lens for mode controlling. A photonic micro-cavity finite difference time domain (FDTD) model had been built to simulate the optical field distribution inside of the cavity of micro-lens integrated VCSEL. The simulation structure is just the same as what is shown in Fig. 1. A dipole source locating inside of the cavity can excite all the modes supported by the cavity [12]. In the simulation, the diameter and the aspherical constant of micro-lens are fixed at 9 $\mu$m and 2 (defined by fitting the data of etched micro-lens profiles according to the formula of the lens profile mentioned in reference [15]), respectively. To simplify the simulation modeling difficulty, the actual multilayer micro-lens is replaced with a homogeneous $GaAs$ aspherical-cap. The active region is keep same as the actual VCSEL structure and contains 3 quantum-wells with gain medium. By changing the heights of the

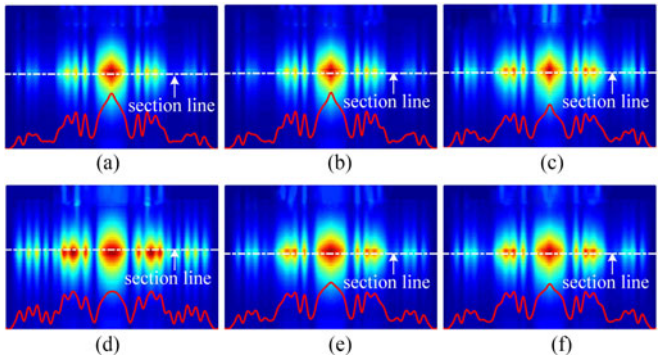


Fig. 2. The simulated internal optical field distribution of the micro-lens integrated VCSELs. The values of $R_c$ are (a) 101.3 $\mu$m (height 100 nm), (b) 67.6 $\mu$m (height 150 nm), (c) 50.7 $\mu$m (height 200 nm), (d) 40.6 $\mu$m (height 250 nm), (e)33.9 $\mu$m (height 300 nm), (f) 29.1 $\mu$m (height 350 nm).

micro-lens, different curvature radius $R_c$ can be obtained. The loss analysis of transverse modes is performed through the photonic micro-cavity model. The variation mirror mode loss of the cavity mode, which is introduced by the non-planar aspheric surface, can distinguish the modes in the cavity. The vertex region of micro-lens experiences much less cavity-loss and the beneath area in the active region suffers from much less gain-loss. The simulation results are shown in Fig. 2. When $R_c$ is larger than 50.7 $\mu$m the ***E***-field concentrates in the center of the cavity, this means that the fundamental mode operation can be achieved. Higher order transverse modes will be excited when $R_c$ decreases down to 40.6 $\mu$m. To realize mode control and high beam quality, a micro-lens with curvature radius less than 40.63 $\mu$m is necessary for prompting the fundamental mode to dominate the optical field in the cavity of micro-lens VCSEL. Therefore, the stable and precise etching process is essential for forming of micro-lens VCSEL.

Monolithically integrated micro-lens VCSELs were fabricated, following to the results of the simulation. To act as a reference, we also made VCSELs without micro-lenses on the identical wafer.

Before the micro-lens etching process, our standard VCSEL fabrication was carried out. After p-contact metallization and lift-off process, an additional lithography was carried out to expose the center area of the VCSEL output window. After development, the leaving unexposed photoresist was served as mask for wet chemical-etching and the 9 $\mu$m circular-hole defined the diameter of the etching window. Then, the patterned wafer was immersed in the wet chemical etchant, a mixture of $H_2O_2$, $HBr$, $CH_3OH$ and $H_2O$ at the ratio of 1:1:1:10 in volume. The spatial variation in the etching rate at the edge and the center region of the circular-hole enabled an aspherical profile on the surface of emitting window to be formed. In our work, the etch rate was slowed down and kept at a steady value in the static undisturbed environment by decreasing the temperature of the mixture liquid, that was came true by putting the beaker with etchant in the ice water and maintaining it for some time. The methanol was added to dissolve the producing $Br_2$ molecular and make it adhere to the etching surface better for smoother etching surface. The etch depth was controlled by etch time [12]–[14]. Thus, micro-lenses with different $R_c$ were directly etched on the uncovered surface.

As is shown in Fig. 3, the etched micro-lenses were measured using optical microscope and an atom force microscope (AFM). The heights of the vertex of the micro-lenses are 182 nm and 348 nm. The diameters of micro-lenses are 9.00 $\mu$m and 9.38 $\mu$m respectively. According to the measured data, the $R_c$ and focus length can be calculated. They are 31.78 $\mu$m and 31.78/(n–1) $\mu$m for higher one and 55.63 $\mu$m and 55.63/(n–1) $\mu$m for lower one, respectively [15].

## 3. Results and Discussions

The *L-I-V* characteristics of the VCSELs were measured at room temperature in continuous wave operation. Fig. 4(a) shows the properties of the conventional VCSEL. Within the range of measuring current, threshold current and maximum output power were found to be 0.9 mA and 4.25 mW,

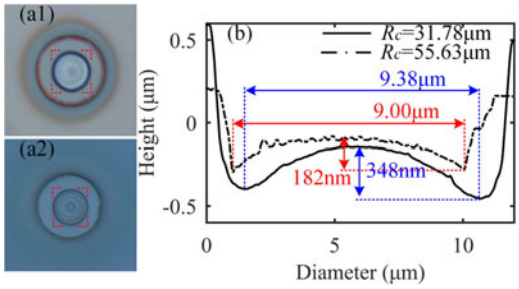


Fig. 3. (a1), (a2) The surface appearance of etched VCSEL measured under optical microscope. (b) Section curves across the vertex of micro-lenses obtained through AFM measuring.

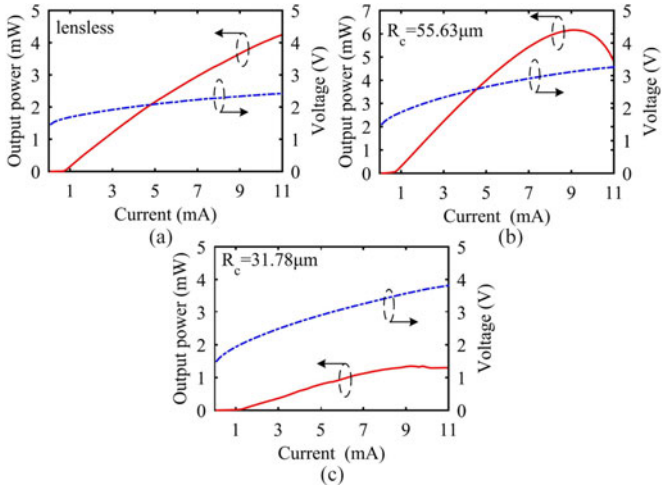


Fig. 4. (a) The *L-I-V* characteristics of conventional VCSELs, (b) VCSEL integrated with $R_c = 55.63\ \mu$m micro-lens, (c) and VCSEL integrated with $R_c = 31.78\ \mu$m micro-lens.

respectively. The threshold current and maximum output power of the VCSEL with a micro-lens of $R_c = 55.63\ \mu$m were 0.8 mA and 6.16 mW. The threshold current and maximum output power of the VCSEL with a micro-lens with $R_c = 31.78\ \mu$m were 1.2 mA and 1.35 mW. In this case, the power output was lower than the VCSELs, with higher thresholds as well. The forward voltage drop of two VCSELs with integrated micro-lens are slightly larger than the one of conventional VCSEL.

The output window of the structured VCSEL has been corroded, and much cavity surface loss is introduced. The cap layer and upper DBRs of VCSEL are divided into large numbers of slices, and the reflectivity of the etched upper DBRs can be calculated by transfer matrix method. The calculation result is shown in Fig. 5(d) and labeled with green squares. The reflectivity of the etched upper DBRs presents periodic variation, and decreases with the increasing etching depth. The increased surface loss of the structured VCSEL results in the increasing of threshold current. On the other hand, the threshold current of the VCSELs with a $R_c = 55.6\ \mu$m micro-lens is less than the conventional one. We explain this behavior with better focusing of the top DBR and therefore reduced optical losses. This was expected from our simulation date presented in Fig. 2. Therefore, we were able to improve the emission power and threshold current at the same time. For two structured VCSELs, there are two reasons to be considered to explain the mild increase in forward voltage drop. The main reason is the impaired contact layers and the existence of undercut in the process of etching, and that results in the increasing in resistance and the forward voltage drop eventually. The second reason is the removed heavily doped layers approaching top-surface. Much more efforts must be made in optimizing the etching process in follow-on work.

The Fig. 5(a), (b) and (c) show the lasing spectra of the three types of VCSELs at 1 mA, 2 mA and 3 mA. We can find that the conventional VCSEL operates with multimode at three levels of

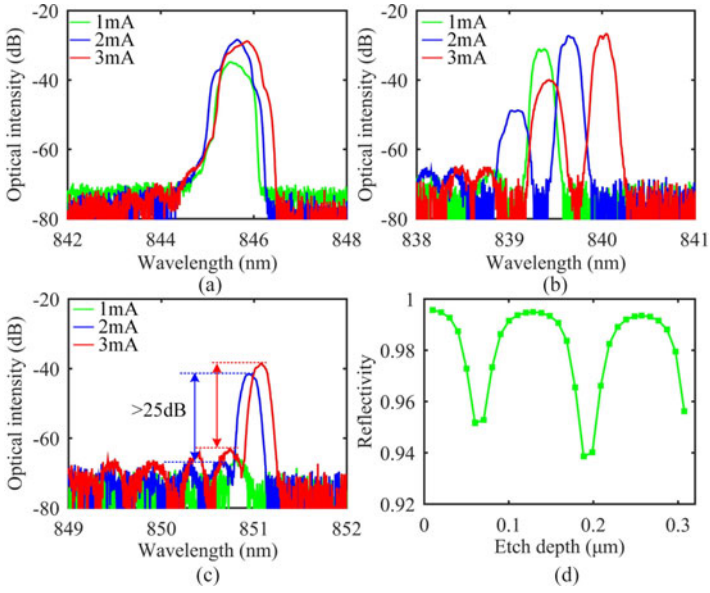


Fig. 5. (a) The spectra of the conventional VCSELs at 1 mA, 2 mA and 3 mA. (b) The spectra of VCSEL with $R_c = 55.63$ $\mu$m micro-lens at 1 mA, 2 mA and 3 mA. (c) The spectra of VCSEL with $R_c = 31.78$ $\mu$m micro-lens at 1 mA, 2 mA and 3 mA. (d) The reflectivity as a function of etch depth assuming a flat profile.

injection currents, and the VCSEL with $R_c = 55.63$ $\mu$m micro-lens can operate in single mode at 1 mA. Nevertheless, it converts single mode into dual mode at higher-level injection currents. Only the VCSEL with $R_c = 31.78$ $\mu$m micro-lens can operate with single mode in the whole range of injection currents and its side-mode suppression ratio (SMSRs) are larger than 25 dB. In addition, we can see that the cavity mode of the VCSELs with $R_c = 55.63$ $\mu$m micro-lens has an emission more blue and the VCSEL with $R_c = 31.78$ $\mu$m micro-lens has an emission more red compared to the reference VCSEL. This is attributed to the different position of the devices on the heterogeneous epitaxial wafer. In addition to that, the phase-condition of the VCSEL device can be slightly different as well. The modal properties of the VCSEL with the $R_c = 31.78$ $\mu$m micro-lens are greatly improved compared to our conventional reference devices and still better than the dual-mode $R_c = 55.63$ $\mu$m micro-lens VCSEL. For the two structured VCSELs, the emission window is corroded and forms a non-planar alike spherical surface. The VCSEL with micro-lens suffers a considerable cavity-surface loss difference between the fundamental mode located at the center of mesa and the high-order modes tended to the edge of the mesa. The threshold gain of the high-order modes is increased dramatically, which suppresses the high-order modes. The VCSEL with smaller curvature radius micro-lens experiences a larger difference than the VCSEL with larger curvature radius. Therefore, the VCSEL with $R_c = 31.78$ $\mu$m lases in single mode with SMSRs $>$ 25 dB. The introduced micro-lens filters out high-order modes of conventional VCSEL successfully, and improves the mode property of the micro-lens VCSEL.

In our simulation, the actual aspherical micro-lens formed by alternating quarter-wavelength thick $Al_{0.12}Ga_{0.88}As/Al_{0.9}Ga_{0.1}As$ layers was displaced by a homogeneous $GaAs$ aspherical-cap. The reflectivity modulation brought in by the $GaAs$ aspherical-cap and DBRs micro-lens exists a mismatch. The small variation in cavity-loss across the entire output window in the simulation results in the poor mode discrimination. As shown in Fig. 2, the intensity of the dominant mode is slightly stronger than side-lobes'. However, for the actual devices with etching micro-lens, the introducing variation in reflectivity on the surface of micro-lens is described in Fig. 5(d). The dramatic change of reflectivity causes enormous mirror- and gain-loss. That makes the mode discrimination possible.

At different injection currents, the far-field patterns of the three types of VCSELs are measured according to the focal length method, and the results are shown in Fig. 6. The VCSEL with the

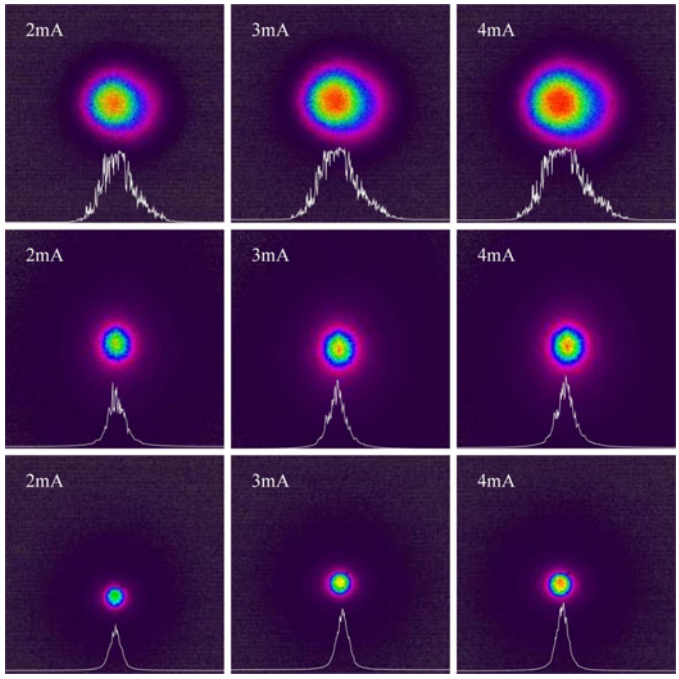


Fig. 6. Far-field distribution measured at 2 mA, 3 mA and 4 mA. The upper figures were for conventional VCSEL, middle ones for VCSEL with 55.63 $\mu$m curvature radius micro-lens the lower ones were for VCSEL with 31.78 $\mu$m curvature radius micro-lens.

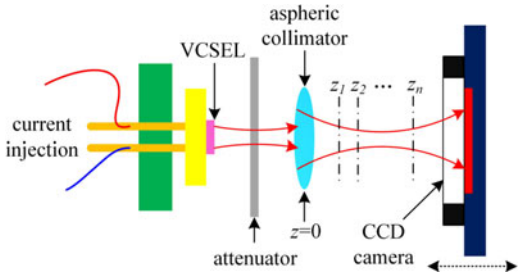


Fig. 7. Schematic diagram of experimental setup for measuring beam quality factor $M^2$. $z_1, z_2, \ldots, z_n$ were the distances away from the lens location $z = 0$.

smallest curvature radius micro-lens displays the smallest beam spots. The divergence angles of conventional VCSEL are 14.5°, 16.0° and 17.0° (full width of $D4\sigma$, where $\sigma$ is the standard deviation of the horizontal or vertical marginal distribution, and the beam width is 4 times $\sigma$.) at 2 mA, 3 mA and 4 mA. At the same injection currents, the divergence angle of VCSEL with $R_c = 55.63$ $\mu$m micro-lens are 8.2°, 8.5° and 9.8°, and the divergence angles of VCSEL with $R_c = 31.78$ $\mu$m micro-lens are reduced to 4.2°, 5.5° and 5.7°. The reflectivity of vertex area of the DBRs micro-lens is larger than the reflectivity of the edge of micro-lens. The feedback light at the center of the aperture is stronger than the feedback at the edge of the aperture, which corresponds to the edge of the micro-lens. The field strength located in the quantum well active layer at the center of the aperture is enhanced and spatially concentrated toward the center of aperture. The smaller curvature radius micro-lens VCSEL experiences a higher level of feedback respect to the VCSEL with larger curvature radius micro-lens, and better compression efficiency is obtained [14], [16]. Therefore, the far-field divergence angles of the VCSEL with $R_c = 31.78$ $\mu$m micro-lens are diminished most distinctly compared to the ones of the other two types of VCSELs.

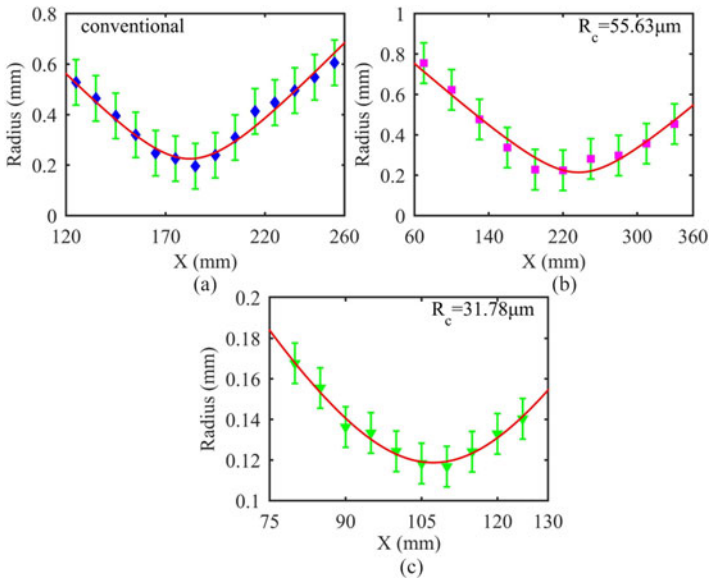


Fig. 8. (a) The beam quality factor $M^2$ of conventional VCSEL, (b) VCSEL with 55.63 $\mu$m curvature radius micro-lens and (c) VCSEL with 31.78 $\mu$m curvature radius micro-lens.

The beam quality factor $M^2$ is measured under available conditions. The Fig. 7 shows a manual experimental test platform for measuring the beam quality factor. An attenuator is inset to attenuate the amplitude of the emitting light. The initial light is collimated by the aspheric collimator lens, and the collimated light is collected by CCD camera. The beam radius can be obtained on the interface of BeamGage software.

The $M^2$ factor depicts the deviation between the ideal Gaussian beam and the practical beam, and the product of waist radius and far-field divergence angle is a constant.

$$W_0\theta = \frac{\lambda}{\pi}M^2 \tag{1}$$

where $W_0, \theta$ are the waist radius and divergence angle. Propagation formula of practical Gaussian beam can be expressed as follows:

$$W(z) = W_0\sqrt{1+\left[\frac{M^2(z-z_0)\lambda}{\pi W_0^2}\right]^2} \tag{2}$$

*W(z)* is the beam radius at different positions, and it is defined by half width of the D4$\sigma$ width of a beam in the horizontal or vertical direction [17], which is more accurate compared with the radius calculated by full width at half maximum (FWHM) and $1/e^2$ width for multimodal marginal distributions. $W_0$ is waist radius at beam waist position $z_0$. $z$ is the distance between the focusing lens and CCD camera. According to the recorded beam spot sizes, the radius of beam spots can be calculated easily. All the measuring parameters and radius of beam spots are substituted into formula (2). The $M^2$ is obtained through Gaussian fitting, in which $M^2$ is a fitting parameter [18].

At 3 mA, the beam radius *W(z)* of the three types of VCSELs at different distance $z$ are measured and the results are shown in Fig. 8. The measured beam radius of the three types of VCSEL are marked with different geometric marks, and the red solid lines are their Gaussian fitted curves. The $M^2$ factor of conventional VCSEL is 6.9, and the $M^2$ factors of the VCSELs with $R_c = 55.63$ $\mu$m and $R_c = 31.78$ $\mu$m micro-lens at 3 mA are reduced to 3.3 and 1.9 respectively. The beam quality factors $M^2$ of the two VCSELs with micro-lens are much smaller than the one of conventional VCSEL. The anisotropic etching in DBRs introduces a great difference of cavity surface loss between the fundamental and high-order modes. The high-order modes located on the edge of the micro-lens

suffer from a larger cavity surface loss, and are weakened. Thus, the fundamental mode located in the center of the mesa is distinguished.

## 4. Conclusion

The cavity surface loss introduced by etching the output window is utilized to filter the high-order mode and distinguish the fundamental mode. The brought strong optical feedback in the vertex area of the non-planar micro-lens enhances the field strength located at the center of the mesa and further results in the collimated beam and narrowed divergence angle. In comparison with the previous works, we make full use of the merits of wet-chemical etching method to fabricate VCSELs integrated with DBR micro-lens economically. Increased single mode power, narrowed divergence angles and improved beam quality can be achieved simultaneously in the monolithic micro-lens VCSEL. In addition, our design can be generalized to VCSELs with different wavelength.

## References

[1] H. Martinsson, J. A. Vukusic, M. Grabberr, and R. Michalzik, "Transverse mode selection in large-area oxide-confined vertical-cavity surface-emitting lasers using a shallow surface relief," *IEEE Photon. Technol. Lett.*, vol. 11, no. 12, pp. 1536–1538, Dec. 1999.
[2] H. Michael, C. Y. Zhou, Y. Chang-Hasnain, and J. Connie, "Single mode high-contrast subwavelength grating vertical cavity surface emitting lasers," *Appl. Phys. Lett.*, vol. 92, no. 17, 2008, Art. no. 171108.
[3] L. J. Mawst, "High-power single-mode antiresonant reflecting optical waveguide-type diode lasers," *Proc. SPIE—Int. Soc. Opt. Eng.*, vol. 20, no. 21, pp. 2219–2221, 1995.
[4] G. E. Giudice, D. V. Kuksenkov, L. G. de Peralta, and H. Temkin, "Single-mode operation from an external cavity controlled vertical-cavity surface-emitting laser," *IEEE Photon. Technol. Lett.*, vol. 11, no. 12, pp. 1545–1547, Dec. 1999.
[5] I. Kardosh, F. Demaria, F. Rinaldi, and S. Menzel, "High-power single transverse mode vertical-cavity surface-emitting lasers with monolithically integrated curved dielectric mirrors," *IEEE Photon. Technol. Lett.*, vol. 20, no. 24, pp. 2084–2086, Dec. 2008.
[6] N. A. Maleev *et al.*, "Single-spatial-mode semiconductor VCSELs with a nonplanar upper dielectric DBR," *Semiconductors*, vol. 47, no. 7, pp. 993–996, 2013.
[7] D.-S. Song, S.-H. Kim, H.-G. Park, C.-K. Kim, and Y.-H. Lee, "Single-fundamental-mode photonic-crystal vertical-cavity surface-emitting lasers," *Appl. Phys. Lett.*, vol. 80, no. 21, pp. 3901–3903, 2002.
[8] H. T. Hsieh, V. Lin, J. L. Hsieh, G. Su, and D. John, "Design and fabrication of long focal length microlens arrays," *Micro Nano Lett.*, vol. 6, no. 7, pp. 523–526, 2011.
[9] Y. Fu, "Integration of microdiffractive lens with continuous relief with vertical-cavity surface-emitting lasers using focused ion beam direct milling," *IEEE Photon. Technol. Lett.*, vol. 13, no. 5, pp. 424–426, May 2001.
[10] Q. S. Li *et al.*, "Direct integration of aspherical microlens on vertical-cavity surface emitting laser emitting surface for beam shaping," *Opt. Commun.*, vol. 300, no. 14, pp. 269–273, 2013.
[11] Il-S. Chung, K. Panajotov, M. Dems, P. Nyakas, S. Bischof, "Numerical methods for modeling photonic-crystal VCSELs," *Opt. Express*, vol. 18, no. 15, pp. 16042–16054, 2010.
[12] E. M. Strzelecka, G. D. Robinson, M. G. Peters, F. H. Peters, and L. A. Coldren, "Monolithic integration of vertical-cavity laser diodes with refractive GaAs microlenses," *Electron. Lett.*, vol. 31, no. 9, pp. 724–725, Apr. 1995.
[13] Y.-S. Kim, J. Kim, J.-S. Choe, Y.-G. Rob, H. Jeon, and J. C. Woo, "Semiconductor microlenses fabricated by one-step wet etching," *IEEE Photon. Technol. Lett.*, vol. 12, no. 5, pp. 507–509, May 2000.
[14] S. Adachi and K. Oe, "Chemical etching characteristics of (001)GaAs," *J. Electrochem. Soc.*, vol. 130, no. 12, pp. 2427–2435, 1983.
[15] P. Nussbaum, R. Vlkel, H. P. Herzig, M. Eisner, and S. Haselbeck, "Design, fabrication and testing of microlens arrays for sensors and microsystems," *Pure Appl. Opt., J. Eur. Opt. Soc. Part A*, vol. 6, no. 6, pp. 617–636, 1997.
[16] S. H. Park, S. Lee, and H. Jeon, "Mode-stabilized operation in a Microlens-Integrated 980 nm vertical-cavity surface-emitting laser," *Opt. Rev.*, vol. 13, no. 3, pp. 146–148, 2006.
[17] M. Dahmen, W. Schulz, V. Kostrykin, and R. Poprawe, "Beam diagnosis and simulation for laser materials processing," in *Proc. Opt. Soc. of Amer.*, 1998, Paper MQ5.
[18] L. Te *et al.*, "Beam quality of 980 nm high power vertical-cavity surface-emitting laser," *Chin. J. Lasere*, vol. 34, no. 5, pp. 641–645, 2009.